A Molecular Jump Mechanism of Water Reorientation

Damien Laage[1]* and James T. Hynes[1,2]*

Despite long study, a molecular picture of the mechanism of water reorientation is still lacking. Using numerical simulations, we find support for a pathway in which the rotating water molecule breaks a hydrogen bond (H-bond) with an overcoordinated first-shell neighbor to form an H-bond with an undercoordinated second-shell neighbor. The H-bond cleavage and the molecular reorientation occur concertedly and not successively as usually considered. This water reorientation mechanism involves large-amplitude angular jumps, rather than the commonly accepted sequence of small diffusive steps, and therefore calls for reinterpretation of many experimental data wherein water rotational relaxation is assumed to be diffusive.

Most of the remarkable properties of liquid water stem from its ability to form dynamic, labile H-bond networks (*1*–*5*) whose connectivity changes constantly, especially because of the rotation of individual water molecules. Water reorientation is of importance in a wide range of processes, including proton transfer (*6*, *7*) and proton transport (*8*, *9*), where it can be the rate-limiting step, and hydration of macromolecules such as proteins, where the water dynamics are essential for protein function (*2*). This reorientation has long attracted experimental interest (*10*), with much very recent activity (*11*–*17*) prompted by progress in time-resolved infrared spectroscopy that now allows detailed study of H-bond dynamics in liquid water. The attained femtosecond time resolution is well adapted to the rapid local structural changes in the H-bond network. Several of these studies (*11*–*15*) have focused on the reorientation kinetics of liquid water or its isotopic variants, extending previous studies based on dielectric relaxation, terahertz (THz) spectroscopy (*17*), optical and Raman-induced Kerr-effect spectroscopy (*16*), nuclear magnetic resonance (NMR) (*16*), and neutron scattering (*10*).

The observed picosecond orientational relaxation of water molecules is usually believed to be related to H-bond breaking and forming, but the specific sequence of events remains unclear. Several mechanisms have been suggested (*1*), involving, e.g., "flickering clusters," which have been argued not to be applicable (*1*), or icelike orientational defects, or especially the Debye small-step diffusion model, but a molecular mechanism consistent with all experimental data is elusive. Although the diffusion model has been most often employed in discussions of water reorientation, several authors (*1*, *2*, *16*, *18*) have expressed doubts about its validity.

It is commonly assumed (*1*, *2*) that to reorient markedly, a water molecule must break at least the H-bond involving the rotating hydrogen. We therefore first focus on the molecular mechanism describing the migration of this H-bond donor site from one accepting water molecule to another. We then show that this exchange phenomenon dominates the observed reorientation dynamics.

Classical molecular dynamics (MD) simulations provide an incisive tool for this study, because they provide a molecular picture of the mechanism while giving results that can be compared with experimental measurements, e.g., from time-resolved infrared spectroscopy. The simulations are performed with 256 H_2O molecules in a periodic cubic box with Ewald summation for long-range forces, employing the rigid simple point charge extended (SPC-E) model to describe the water molecules, with a 0.5-fs timestep. This computational scheme and model have been shown to yield good agreement with experimental results (*12*, *14*, *18*).

To detect H-bond breaking and forming events along a dynamical trajectory, criteria characterizing the existence of an H-bond must first be chosen. We have adopted the widely used geometric definition (*5*, *12*, *19*, *20*): $R_{OO} < 3.5$ Å, $\theta_{HOO} < 30°$, where R_{OO} is the distance between the donor and acceptor oxygen atoms, and θ_{HOO} is the angle between the OH bond and the OO vectors.

After a 50-ps equilibration period at 300 K and a density of 1 g/cm^3, a 75-ps classical MD trajectory for pure H_2O is generated in the microcanonical ensemble. We record all the times when a hydrogen atom changes the acceptor oxygen with which it forms an H-bond and collect more than 16,000 such H-bond "switches"; these switches are a feature common to all water molecules, i.e., they do not represent a subensemble. The switching comprises three steps: (i) the breaking of an initial H-bond formed between two water molecules $HO^*\text{-}H^*\cdots O^aH_2$; (ii) the rotation of the hydrogen H* on the central water molecule; and (iii) the formation of a new H-bond with a different water molecule $HO^*\text{-}H^*\cdots O^bH_2$. We select all the sequences in the trajectory occurring before and after a switching event, provided that H* is H-bonded to either O^a for $t < 0$ or to O^b for $t > 0$ (because near $t \approx 0$, the $O^aO^*H^*$ and $O^bO^*H^*$ angles are close to 30°, the H-bond criteria for the definition of this ensemble are extended to $R_{OO} < 4.0$ Å, $\theta_{HOO} < 50°$). Then we calculate the average over the different trajectories of the time evolution for different key quantities (Fig. 1).

We monitor the oxygen-oxygen distances R_{O^*Oa} and R_{O^*Ob}, together with the angle θ between the projection of the O*H* vector on the $O^*O^aO^b$ plane and the $O^aO^*O^b$ angle bisector (Fig. 2). This definition of θ renders it independent of both any motion of H* out of the $O^*O^aO^b$ plane and any $O^aO^*O^b$ bending. When $\theta = 0°$, H* is equidistant from O^a and O^b.

From more than 16,000 averaged successful trajectories, the flipping of H* from O^a toward

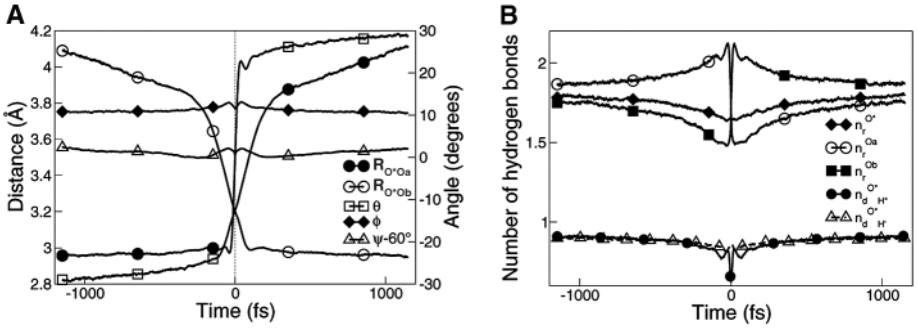

Fig. 1. Time evolution, centered on the H-bond switching event, of (**A**) different geometric quantities and (**B**) the number of H-bonds. (A) R_{O^*Oa}, R_{O^*Ob} distances and θ angle defined in text and Fig. 2; ϕ is the out-of-plane angle between the O*H* bond and the $O^*O^aO^b$ plane; ψ is the $O^aO^*O^b$ angle, shifted by 60°. θ oscillations between $t \approx -100$ fs and $t \approx +100$ fs arise from the coherent averaging of the trajectories centered on $t = 0$ when $\theta = 0$. The period is ~140 fs, about twice that associated with the water 440 cm^{-1} librational band (*10*), consistent with an angular range about double the appropriate range in either the reactant or product H-bonding conformation. (B) $n_r^{O^*}$, n_r^{Oa} and n_r^{Ob} are the numbers of H-bonds accepted, respectively, by O*, O^a, and O^b; $n_d^{O^*}{}_{H'}$ and $n_d^{O^*}{}_{H^*}$ are the numbers of H-bonds donated by O* through its H′ and H* hydrogens, respectively. O^a for $t \ll 0$ and O^b for $t \gg 0$ are more coordinated than the average bulk oxygen, because H* is always H-bonded to either O^a or O^b in the configurations contributing to the average.

[1]CNRS UMR 8640 Pasteur, Département de Chimie, Ecole Normale Supérieure, 24 rue Lhomond, 75231 Paris Cedex 05, France. [2]Department of Chemistry and Biochemistry, University of Colorado, Boulder, CO 80309–0215, USA.

*To whom correspondence should be addressed. E-mail: damien.laage@ens.fr (D.L.); hynes@chimie.ens.fr (J.T.H.)

O^b occurs in approximately 250 fs, on average from $\theta = -29°$ to $\theta = +29°$. The actual angular jump only takes place once the two oxygen atoms O^a and O^b are equidistant from O*: $R_{O^*O^a} = R_{O^*O^b}$ (Fig. 1). The θ angle is therefore a fast coordinate that adapts rapidly to the environment. The rotation of H* occurs nearly within the $O^*O^aO^b$ plane, because the angle ϕ between the O*H* direction and the $O^*O^aO^b$ plane remains approximately constant and equal to 11°. The other H-bonds involving O* remain intact during the rotation: The H-bond donated by the other hydrogen, labeled H′, attached to O*, is unaffected, and the two H-bonds accepted by O* are only slightly weakened (Fig. 1).

By following the averaged trajectories backward in time from the midpoint $t = 0$, defined by $\theta = 0$, we see why the condition $R_{O^*O^a} = R_{O^*O^b}$ occurs. The trajectories show that, before reaching the situation where $R_{O^*O^a} = R_{O^*O^b}$, O^a is H-bonded to H* and lies in the O* first hydration shell ($R_{O^*O^a} \approx 2.95$ Å), whereas O^b is initially located on the inner side of the O* second hydration shell ($R_{O^*O^b} \approx 4.1$ Å). Both O^a and O^b accept $n^{bulk} \approx 1.8$ H-bonds, as does any water molecule in the bulk on average. The departure of O^a away from O* and the motion of O^b toward O* are initiated by changes in the numbers of H-bonds accepted by O^a and O^b as a result of fluctuations in the bulk H-bond network. The coordination of O^a increases markedly, by close to 0.3 in excess of n^{bulk} H-bonds, and therefore O^a moves away from the H-bond donated by H*. In contrast, the coordination of O^b drops by approximately –0.3 from n^{bulk}, attracting O^b toward H* to regain coordination. This difference in coordination is at the origin of the motion of O^a and O^b, leading to the $R_{O^*O^a} = R_{O^*O^b}$ conformation, where the H* rotation takes place; it is also analogous to the slow environment reorganization coordinate that has been put forward as the reaction coordinate for proton transfers in solution (*7*).

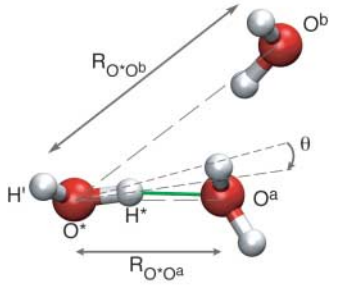

Fig. 2. Scheme of the different geometric coordinates. $R_{O^*O^a}$ and $R_{O^*O^b}$ are the oxygen-oxygen distances between the rotating water and the initial and final H-bond acceptor, respectively. θ is the angle between the projection of the O*H* vector on the $O^*O^aO^b$ plane and the bisector of the $O^aO^*O^b$ angle. All dashed lines lie within the $O^*O^aO^b$ plane.

The different stages of our computed mechanism are represented schematically in Fig. 3. This molecular mechanism indicates that the reorientation of a water molecule occurs by large amplitude rotations, or jumps. The O*-H* direction oscillates around the O*-H*···O^a H-bond axis until collective fluctuations of the H-bond network (*3*) reorganize the environment in such a way that when H* rotates out of the H-bond with O^a, it can immediately form a new H-bond with O^b, thus lowering the energy cost associated with the H-bond breaking. As stressed above, the two coordination number changes are key in this reorganization. The first step in the reorientation is, therefore, the formation of an H-bond around O^a and the cleavage of an H-bond around O^b in the second hydration shell around the rotating water. This result contradicts a standard assumption, namely that the first step is instead the breaking of the H-bond such that a dangling, i.e., non–H-bonded, O*H* is formed, which will subsequently reorient (*1*, *2*). The very recently established unstable character of the dangling H-bond in fact leaves little time for such subsequent reorientation (*20*).

In the present mechanism, an unstable dangling O*H* does not appear. Instead, the key unstable structure is that of the transition state, whose structure exhibits a bifurcated H-bond, with a five-coordinate rotating water (*21*). This last result confirms previous findings that five-coordinate water molecules have higher translational and rotational mobility (*22*), and it provides the molecular mechanism for the formation of these defects. In addition, such a jump mechanism for water rotation is in strong contrast with the diffusive reorientation commonly assumed in the interpretation of time-resolved infrared (*13*–*15*), Raman-induced Kerr-effect (*16*), NMR (*16*) or THz (*17*) spectroscopies, and neutron-scattering experiments (*10*). It also differs from the mechanism determined in isolated water clusters (*23*) because of the constraints imposed by the H-bond network in the bulk. Although the reorientation mechanism suggested in ice (*1*) also involves large angular jumps, it strongly differs from the present mechanism, because the rotating water keeps the same neighbors in its tetrahedral environment and the D/L orientational defects diffuse independently, whereas here the reorientation requires an overcoordinated/undercoordinated defect pair around the rotating water.

Our proposed mechanism can be related to the orientational relaxation times obtained from experiments or MD simulations through the jump model developed by Ivanov (*24*). The water molecule is approximated as spherical so that rotations about different axes occur with the same probability [although water rotation is anisotropic, the OH rotational diffusion constant is close to the averaged isotropic rotational diffusion constant (*25*)]. The molecular orientation is assumed to be "frozen" between changes induced by instantaneous constant-amplitude orientation jumps. Two parameters apply in this model, the first being the average amplitude of the rotational jumps, which we determined to be $\theta_0 = 60°$ from the average $O^aO^*O^b$ angle when the jump occurs (Fig. 1). Because the O*-H* bond oscillates in the direction of O^a for $t < 0$ and in the direction of O^b for $t > 0$, the $O^aO^*O^b$ angle at $t = 0$ gives the angular jump amplitude

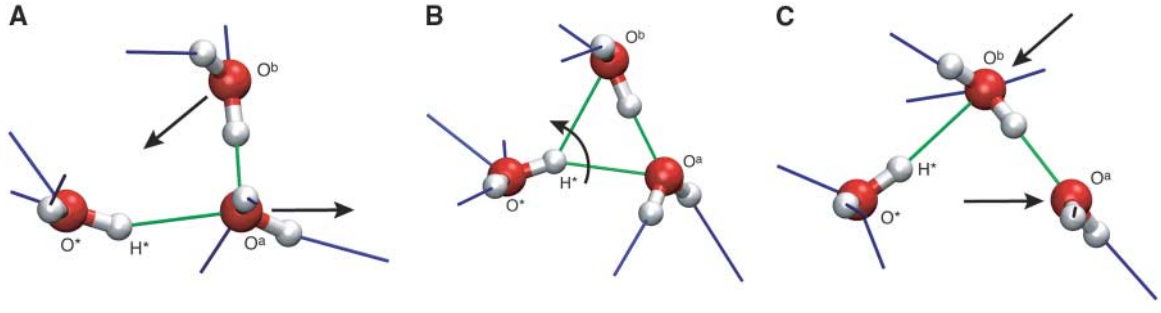

Fig. 3. Scheme of the different steps in the computed H-bond exchange mechanism. Each frame is a snapshot of an actual H-bond switching event in the simulations. The green sticks designate the H-bonds within the O*, O^a, O^b water trimer, and the blue sticks represent the H-bonds between the trimer and the surrounding water molecules, which are not shown. The black arrows show the key motions. (**A**) H* is H-bonded to O^a in its first hydration shell, with O^b farther away in the second hydration shell; because of collective fluctuations in the H-bond network, O^a is overcoordinated, whereas O^b is undercoordinated. This conformation leads to the O^a motion away from O* and O^b motion toward O*. The configuration displayed here with O^a and O^b H-bonded occurs in ~60% of the observed switches. (**B**) O^a and O^b are equidistant from O*, and H* flips from O^a toward O^b; O^a and O^b have the same coordination number. (**C**) O^b forms an H-bond with H* and becomes overcoordinated, whereas O^a has lost an H-bond and is now undercoordinated; the trimer is in a situation similar to (A), with O^a and O^b interchanged; fluctuations of the H-bond network will allow the configuration to relax to equilibrium.

$\theta_0 = 60°$; Fig. 1 shows that the average $O^aO^*O^b$ angle varies little during the switch.

The second parameter is the frequency $1/\tau_0$ of these jumps, which corresponds to the rate constant of the H-bond switching event that we have monitored. This rate constant is extracted from our simulations by calculating the correlation function $[1 - \langle n_a(0) n_b(t)\rangle]$, where n_a is 1 when H* is H-bonded to O^a and 0 otherwise, and n_b is 1 when H* is H-bonded to O^b and 0 otherwise. In addition, absorbing conditions are used for n_b so that when a new H-bond has formed, it remains intact. We thus discard any contribution from the back reaction or from the subsequent rupture of the O^b H-bond, so that the extracted time is associated with the forward rate constant for the H-bond switching (*19*). This correlation function exhibits a mono-exponential decay with a characteristic time $\tau_0 = 1.8$ ps (Fig. 4A). The Ivanov jump model then provides the τ_n^{jump} characteristic times associated with the different rotational correlation functions $\langle P_n[\mathbf{u}_{OH}(0)\cdot\mathbf{u}_{OH}(t)]\rangle$ where P_n is the nth order Legendre polynomial and $\mathbf{u}_{OH}$ the direction of the rotating OH bond

$$\tau_n^{jump} = \tau_0 \Big/ \left(1 - \frac{1}{2n+1}\,\frac{\sin(n+1/2)\theta_0}{\sin\theta_0/2}\right) \quad (1)$$

If the angular jump is very small, this relation reduces to the diffusive reorientation case $\tau_n^{dif} = 1/[n(n+1)D_{OH}]$, with the OH rotational diffusion coefficient $D_{OH} = \theta_0^2/6\tau_0$.

As noted above, the Ivanov jump model assumes that the O*-H* orientation is "frozen" between jumps. Figure 4B displays the orientation correlation functions calculated over all the trajectories during the time intervals between two successive H-bond switches and indicates that there is instead a relatively slow reorientation process occurring between jumps (compare with Fig. 4A). Figure 4B shows that this slow reorientation can be understood in terms of the coupling of the OH* to the OO axis in the initially H-bonded pair, which will be shown below to be diffusive in character. To incorporate this slower process in our description within an extended jump model, we can employ the relation (*26*) for orientation correlations involving several statistically independent reorientation sources

$$\langle P_n(\mathbf{u}_{OH}(0)\cdot\mathbf{u}_{OH}(t))\rangle = \langle P_n(\hat{\mathbf{u}}_{OH}(0)\cdot\hat{\mathbf{u}}_{OH}(t))\rangle \times \langle P_n(\mathbf{u}_{OO}(0)\cdot\mathbf{u}_{OO}(t))\rangle \quad (2)$$

in the present case connecting the orientational correlation functions to those for the OO axis frame and for the "internal" switch. Here $\hat{\mathbf{u}}_{OH}$ is the direction of the rotating OH bond in the OO frame, and $\mathbf{u}_{OO}$ is the direction of the OO axis in the laboratory frame. Because, from Fig. 4, each of the latter functions is exponential in time past a very short transient period (~400 fs), the time dependence of the nth Legendre polynomial is exponential, with a decay time given by

$$\frac{1}{\tau_n} = \frac{1}{\tau_n^{jump}} + \frac{1}{\tau_n^{OO}} \quad (3)$$

where τ_n^{OO} is the exponential decay time associated with the OO frame between jumps determined from the simulation results in Fig. 4B.

Table 1 summarizes the different values obtained for the orientational relaxation times, either from experiments (if available), from our MD simulations, from the diffusive model with the OH rotational diffusion constant calculated from our MD simulations independently of any consideration of the jumps (*25*), from jump model calculations using the θ_0 and τ_0 values determined by the simulations, from the OO frame rotational reorientation between H-bond switches, or from the extended jump model combining jumps and OO reorientation. The MD results are shown to be fully consistent with the available experimental relaxation time values. The calculated τ_2 value is 2.0 ps, in agreement with the 1.7 to 2.6 ps range of values obtained from different experimental techniques (*12*, *13*, *15*, *16*), thus validating our method. Inspection of the τ_n values predicted by the OH diffusive model shows very poor agreement with both the experiments and the MD simulations; the standard diffusive value of 3 for the τ_1/τ_2 ratio agrees only very approximately with the MD ratio of 2.1, which has been in the past considered to be sufficient for a confirmation of the diffusive behavior. Regarding the extended jump model, the explicit inclusion of the OO reorientation between jumps shortens only slightly the predicted reorientation times of the simple jump model, because the reorientation is dominated by the fast jumps with respect to the slow OO reorientation. (The values of the τ_1/τ_2 and τ_1/τ_3 ratios of 3.0 and 5.5 for the latter OO reorientation tend to indicate a diffusive process for it.) For the τ_n values given by the extended jump model, the agreement with the MD results is now excellent, and the predicted τ_1/τ_2 ratio of 2.5 is in better agreement with the MD results than the diffusive ratio.

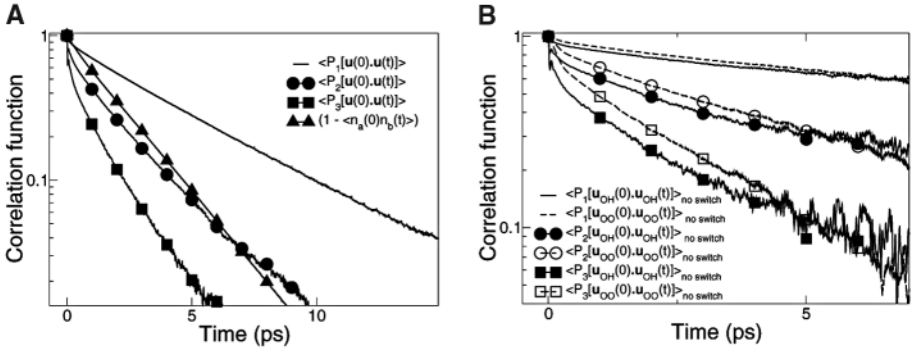

Fig. 4. Orientational and H-bond correlation functions. (**A**) The orientation correlation functions $\langle P_n[\mathbf{u}_{OH}(0)\cdot\mathbf{u}_{OH}(t)]\rangle$, where P_n is the n^{th} order Legendre polynomial and $\mathbf{u}_{OH}$ the rotating OH bond direction, are calculated with the ensemble of all OH bonds from MD simulation. The slope of the $[1 - \langle n_a(0)\, n_b(t)\rangle]$ correlation function provides the H-bond switching rate; the extracted time for a completed switch is longer than that associated with transient H-bond breaking and making (*5*). (**B**) Orientational correlation functions calculated during the time intervals between two successive H-bond switches, for the OH direction and for the OO direction.

Table 1. Comparison of orientational relaxation times from different sources. τ_D is the Debye relaxation time. The τ_n times (excluding τ_D) were extracted from the present MD simulations by an exponential fit of the long-time component of the correlation function (Fig. 4), which eliminates the fast librational decay that is described by neither the jump nor the diffusive models. The single molecule relaxation time τ_1 cannot be directly determined experimentally but can be inferred by (approximate) dielectric relaxation theory models from τ_D, which include collective motions. Depending on the model used, a τ_1 value between 2 and 7.5 ps can be supported (*2*, *29*, *30*); to our knowledge, the τ_3 time for water has not yet been measured (*27*).

Source of τ values	τ_D (ps)	τ_1 (ps)	τ_2 (ps)	τ_3 (ps)	τ_1/τ_2	τ_1/τ_3
Molecular dynamics	9.7*	4.3	2.0	1.3	2.1	3.3
OH diffusion ($D_{OH} = 0.45$ ps^{-1})	–	1.1	0.4	0.2	3.0	6.0
Jump model ($\theta_0 = 60°$, $\tau_0 = 1.8$ ps)	–	5.4	2.2	1.6	2.4	3.4
OO reorientation between switches	–	15.5	5.2	2.8	3.0	5.5
Extended jump model (Eq. 3)	–	4.0	1.6	1.0	2.5	4.0
Experiment	8.5†	2–7.5‡	1.7–2.6§	–	–	–

*(*18*) †(*17*) ‡(*2*, *29*, *30*) §(*12*, *13*, *15*, *16*)

Examination of the τ_1/τ_3 ratio provides an even clearer picture; this ratio is calculated to be 3.3 from the MD simulations, in good agreement with the extended jump model prediction of 4.0, whereas the purely diffusive model yields a value of 6 (*27*).

Therefore the extended jump model, whose parameters are determined in the accompanying simulations, is shown to be fully consistent with the experimental reorientation times and is clearly supported by MD simulations. These results thus call for a reinterpretation of the many experimental data for which water rotation is assumed to be purely diffusive in character.

Further confirmation of the molecular mechanism presented here could emerge from the resolution of the remaining controversial issues for water reorientation, such as the experimental isotope effect in the reorientation times (*15*), and a possible laser OH excitation frequency dependence of the reorientation times (*12*, *13*, *15*) and angular displacement (*28*).

References and Notes

1. D. Eisenberg, W. Kauzmann, *The Structure and Properties of Water* (Oxford Clarendon, London, 1969).
2. B. Bagchi, *Chem. Rev.* **105**, 3197 (2005).
3. I. Ohmine, H. Tanaka, *Chem. Rev.* **93**, 2545 (1993).
4. C. J. Fecko, J. D. Eaves, J. J. Loparo, A. Tokmakoff, P. L. Geissler, *Science* **301**, 1698 (2003).
5. R. Rey, K. B. Møller, J. T. Hynes, *J. Phys. Chem. A* **106**, 11993 (2002).
6. K. Ando, J. T. Hynes, *J. Mol. Liq.* **64**, 25 (1995).
7. K. Ando, J. T. Hynes, *Adv. Chem. Phys.* **110**, 381 (1999).
8. D. Marx, M. E. Tuckerman, J. Hutter, M. Parrinello, *Nature* **397**, 601 (1999).
9. N. Agmon, *Chem. Phys. Lett.* **244**, 456 (1995).
10. S. H. Chen, J. Teixeira, *Adv. Chem. Phys.* **64**, 1 (1986).
11. S. Woutersen, U. Emmerichs, H. J. Bakker, *Science* **278**, 658 (1997).
12. C. P. Lawrence, J. L. Skinner, *J. Chem. Phys.* **118**, 264 (2003).
13. H. S. Tan, I. R. Piletic, M. D. Fayer, *J. Chem. Phys.* **122**, 174501 (2005).
14. C. J. Fecko, J. J. Loparo, S. T. Roberts, A. Tokmakoff, *J. Chem. Phys.* **122**, 054506 (2005).
15. Y. L. A. Rezus, H. J. Bakker, *J. Chem. Phys.* **123**, 114502 (2005).
16. K. Winkler, J. Lindner, H. Bürsing, P. Vöhringer, *J. Chem. Phys.* **113**, 4674 (2000).
17. C. Rønne, P. O. Åstrand, S. R. Keiding, *Phys. Rev. Lett.* **82**, 2888 (1999).
18. D. van der Spoel, P. J. van Maaren, H. J. C. Berendsen, *J. Chem. Phys.* **108**, 10220 (1998).
19. A. Luzar, D. Chandler, *Nature* **379**, 55 (1996).
20. J. D. Eaves *et al.*, *Proc. Natl. Acad. Sci. U.S.A.* **102**, 13019 (2005).
21. In Csajka and Chandler's paper on some aspects of H-bond breaking in water (as opposed to reorientation), jumps occur in producing a predefined broken H-bond final state, which is an unstable state, without a new partner in most cases and with the former accepting water still in the first hydration shell (*31*). This process is to be distinguished from that of the present work, where jumps terminate in a new stable state, with a new partner, and with the former partner now in the second hydration shell (Fig. 1).
22. F. Sciortino, A. Geiger, H. E. Stanley, *Nature* **354**, 218 (1991).
23. F. N. Keutsch, R. J. Saykally, *Proc. Natl. Acad. Sci. U.S.A.* **98**, 10533 (2001).
24. E. N. Ivanov, *Sov. Phys. JETP* **18**, 1041 (1964).
25. I. M. Svishchev, P. G. Kusalik, *J. Phys. Chem.* **98**, 728 (1994).
26. A. Szabo, *J. Chem. Phys.* **81**, 150 (1984).
27. The τ_3 time is currently available only through MD simulations, but promising time-resolved hyper-Rayleigh scattering techniques should allow its determination for water in the near future (*32*).
28. G. Gallot *et al.*, *J. Chem. Phys.* **117**, 11301 (2002).
29. A. Wallqvist, B. J. Berne, *J. Phys. Chem.* **97**, 13841 (1993).
30. P. Madden, D. Kivelson, *Adv. Chem. Phys.* **56**, 467 (1984).
31. F. S. Csajka, D. Chandler, *J. Chem. Phys.* **109**, 1125 (1998).
32. T. Buckup, personal communication.

33. This work has been supported by the CNRS and NSF grant CHE-0417570.

2 November 2005; accepted 12 January 2006
Published online 26 January 2006;
10.1126/science.1122154
Include this information when citing this paper.

The Role of Pair Dispersion in Turbulent Flow

Mickaël Bourgoin,[1] Nicholas T. Ouellette,[2] Haitao Xu,[2,3] Jacob Berg,[4] Eberhard Bodenschatz[2,3]*

Mixing and transport in turbulent flows—which have strong local concentration fluctuations—are essential in many natural and industrial systems including reactions in chemical mixers, combustion in engines and burners, droplet formation in warm clouds, and biological odor detection and chemotaxis. Local concentration fluctuations, in turn, are intimately tied to the problem of the separation of pairs of fluid elements. We have measured this separation rate in an intensely turbulent laboratory flow and have found, in quantitative agreement with the seminal predictions of Batchelor, that the initial separation of the pair plays an important role in the subsequent spreading of the fluid elements. These results have surprising consequences for the decay of concentration fluctuations and have applications to biological and chemical systems.

Turbulent mixing of liquids and gasses is ubiquitous in nature (*1*); it is the basis of all industrial fluid mixing processes, and it determines the spread of pollutants or bioagents in the atmosphere (*2*) and oceans (*3*). Biological organisms in marine ecosystems also exploit it for their survival (*4*–*6*). A crucial component of turbulent mixing is the fluctuation of local concentration. The rate of destruction of ozone in the atmosphere, for example, is largely determined by these fluctuations rather than by the mean concentration (*7*), as is the toxicity of gas leaks or air pollution. It is natural to relate these concentration fluctuations to the separation of two nearby fluid elements; i.e., pair dispersion (*8*, *9*).

In a quiescent fluid, the relative dispersion of two fluid elements (or tracer particles) is dominated by diffusion. The particles undergo Brownian motion, and the mean square separation between them grows linearly in time. In a turbulent flow, however, if the two particles are separated by distances smaller than the characteristic size of the largest eddies in the flow, they will separate faster (superdiffusively). At large separation times and distances, the local correlations responsible for the superdiffusive separation will no longer be present, and, on average, the relative dispersion will again be linear in time.

Despite almost 80 years of scientific inquiry into relative dispersion (*2*, *9*–*17*), no clear experimental verification of the theoretical predictions has emerged. One critical unresolved question is the extent to which the initial separation of the fluid particles influences their subsequent motion. Our measurements in a laboratory water flow (*18*, *19*) in very intense turbulence suggest that the initial separation remains important for all but the most violent flows on Earth. This observation has consequences for such varied problems as pollution control; combustion modeling; hazardous chemical control; and even the understanding of how animals locate food, predators, and mates (*5*, *6*).

We measured relative dispersion in a water flow at high turbulence levels by using optical particle tracking. This technique has been used for a number of years in turbulence research (*13*, *20*) but was limited to the measurement of low–turbulence level flows, because tracer-particle motions must be resolved over times comparable to the smallest time scale of the turbulence [i.e., the Kolmogorov time scale $\tau_\eta = (\nu/\varepsilon)^{1/2}$, where ν is the kinematic viscosity and ε is the energy dissipation rate per unit mass]. In intense turbulence, these times are often very small. The turbulence level is generally quantified by the Reynolds number, which measures the ratio of the nonlinear inertial forces to the linear viscous forces. Here we report the Reynolds number based on the Taylor microscale, $R_\lambda = \sqrt{(15u'L/\nu)}$,

[1]Laboratoire des Écoulements Géophysiques et Industriels–CNRS (Unité Mixte de Recherche 5519), Boite Postale 53-38041, Grenoble Cedex 9, France. [2]Laboratory of Atomic and Solid State Physics, Cornell University, Ithaca, NY 14853, USA. [3]Max Planck Institute for Dynamics and Self-Organization, Göttingen, Germany. [4]Risø National Laboratory, DK-4000 Roskilde, Denmark.

*To whom correspondence should be addressed. E-mail: eberhard.bodenschatz@ds.mpg.de

A Molecular Jump Mechanism of Water Reorientation

Damien Laage and James T. Hynes

Science **311** (5762), 832-835.
DOI: 10.1126/science.1122154originally published online January 26, 2006